Vacuum ultraviolet excitation of $^1S_0$ and $^3P_0$ emission of Pr^{3+} in $Sr_{0.7}La_{0.3}Al_{11.7}Mg_{0.3}O_{19}$ and SrB_4O_7

2001 J. Phys.: Condens. Matter 13 5471

(http://iopscience.iop.org/0953-8984/13/23/306)

INSTITUTE OF PHYSICS PUBLISHING JOURNAL OF PHYSICS: CONDENSED MATTER

J. Phys.: Condens. Matter **13** (2001) 5471–5486 www.iop.org/Journals/cm PII: S0953-8984(01)20986-2

Vacuum ultraviolet excitation of $^1S_0$ and $^3P_0$ emission of Pr^{3+} in $Sr_{0.7}La_{0.3}Al_{11.7}Mg_{0.3}O_{19}$ and SrB_4O_7

E van der Kolk[1], P Dorenbos and C W E van Eijk

Interfaculty Reactor Institute, Delft University of Technology, Mekelweg 15, 2629 JB Delft, The Netherlands

E-mail: vdkolk@iri.tudelft.nl (E van der Kolk)

Received 16 January 2001, in final form 9 April 2001

Abstract

The emission and excitation properties of a SrB_4O_7:1% Pr^{3+} powder sample and a $Sr_{0.7}La_{0.3}Al_{11.7}Mg_{0.3}O_{19}$:3.5% Pr^{3+} single crystal were investigated using x-ray and synchrotron radiation. The 4f5d states of Pr^{3+} in these host lattices are at a higher energy than the $4f^2[^1S_0]$ state. In the hexa-aluminate this results in the successive emission of two photons. $^1S_0 \rightarrow {}^1I_6$ emission is followed by emission from the $^3P_0$ state. The quantum efficiency of the total $^3P_0$ emission is 25%. In the tetra-borate the $^3P_0$ emission is quenched by multiphonon relaxation to the $^1D_2$ state from which only weak emission is observed. In the hexa-aluminate as in the tetra-borate, host lattice excitation does not result in efficient emission from the $^1S_0$ state. In the hexa-aluminate the excitation energy is transferred from the host lattice preferentially to the lower-energy ^3P_J and $^1I_6$ states, resulting in $^3P_0$ emission only.

1. Introduction

In plasma display panels (PDPs) and Hg-free lighting tubes, phosphors are excited by the vacuum ultraviolet emission (150–180 nm) from a discharge in a noble-gas mixture of Xe and Ne [1]. The high energy of the VUV photons (7–8 eV) relative to the visible (2–3 eV) photons together with the low energy efficiency (10–20%) of the discharge, result in an inefficient emissive device. The high energy of the photons does however allow for the possibility of the emission of two visible photons for each absorbed VUV photon. This photon cascade emission (PCE) or quantum splitting phenomenon was demonstrated in the Pr^{3+}-doped fluorides YF_3, LaF_3, and $NaYF_4$ twenty five years ago [2–4]. In these host lattices the lowest-energy 4f5d state of Pr^{3+} has a higher energy than the $4f^2[^1S_0]$ state and emission can take place in two steps via the transitions $^1S_0 \rightarrow ({}^1I_6, {}^3P_J)$ followed by $^3P_0 \rightarrow ({}^3F_J, {}^3H_J)$ or $^1S_0 \rightarrow {}^1D_2$ followed by $^1D_2 \rightarrow {}^3H_J$ (see figure 1).

Recently the phosphors $LiGdF_4$:Eu^{3+} [5] and $LiGdF_4$:Er^{3+}, Tb^{3+} [6], utilizing combinations of rare-earth ions, showed efficient quantum splitting. Fluorides however are

[1] Author to whom any correspondence should be addressed. Fax: 31-15-2786422.

0953-8984/01/235471+16$30.00

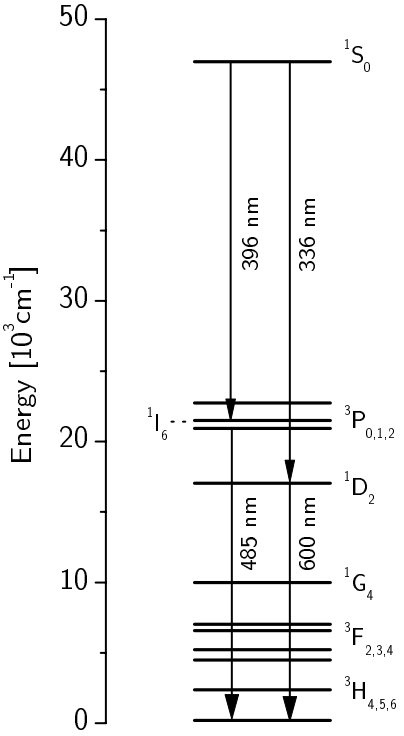

Figure 1. The energy level scheme of Pr^{3+}. The vertical arrows indicate the strongest emission transitions from the $^1S_0$, $^3P_0$, $^4D_2$ states.

generally considered to be unstable and no lighting or display application makes use of a fluoride phosphor [7]. Although it is not certain whether a fluoride is unstable in the VUV applications mentioned above, oxides are preferred above fluorides. Pr^{3+}-based PCE in oxides was discovered four years ago in Pr^{3+}-doped $SrAl_{12}O_{19}$ [8], $LaMgB_5O_{10}$ [9], and LaB_3O_6 [10] although $^1S_0$ emission was observed earlier in the sulphates $Gd_2(SO_4)_3$ [11] and $LiNH_4SO_4$ [12]. A systematic investigation of the PCE process in different sulphates is presented by us elsewhere [13].

The excitation of a Pr^{3+}-doped fluoride by the Xe-discharge emission takes place in the 4f5d configuration of Pr^{3+} since the fluoride host lattice itself is transparent in the 150–180 nm spectral region. Oxides (silicates, aluminates, borates) on the other hand do absorb efficiently in this spectral region and a considerable portion of the Xe-discharge emission is not absorbed by the Pr^{3+} ions but by the host lattice. This requires an efficient energy transfer from the host lattice to the $^1S_0$ state of the Pr^{3+} ion.

In this work the PCE and VUV excitation characteristics of Pr^{3+}-doped SrB_4O_7 and $Sr_{0.7}La_{0.3}Al_{11.7}Mg_{0.3}O_{19}$ are reported and discussed. Synchrotron radiation facilities in addition to our laboratory VUV spectrophotometer were used. It will be demonstrated that the energy transfer from the host lattice to the $^1S_0$ state is inefficient in both host lattices.

The SrB_4O_7 host lattice was selected because the $^1S_0$ type of Pr^{3+} emission was expected. This expectation was based on the Eu^{2+} [14] and Ce^{3+} [15] luminescence in SrB_4O_7. It was recently demonstrated by van der Kolk *et al* [16] that Eu^{2+}-doped host lattices with $^6P_{7/2}$ Eu^{2+} line emission will most probably also show Pr^{3+} $^1S_0$ emission when Pr^{3+} enters the same site as Eu^{2+}. Meijerink *et al* [14] observed $^6P_{7/2} \rightarrow {}^8S_{7/2}$ line emission of Eu^{2+} in the SrB_4O_7 host lattice. Furthermore, using the energy difference of 12 240 cm^{-1} between the Ce^{3+} and Pr^{3+} lowest 5d levels and the observed Ce^{3+} 4f $\rightarrow$ 5d energy of 35 700 cm^{-1} (280 nm) [15],

the lowest Pr^{3+} $4f^2 \rightarrow 4f5d$ energy is predicted at 47 900 cm^{-1} (208 nm) which is at a higher energy than the $^1S_0$ state. This value compares well with the value of 210 nm that is actually found in this work.

$Sr_{0.7}La_{0.3}Al_{11.7}Mg_{0.3}O_{19}$ was selected on the basis of the PCE observed in $SrAl_{12}O_{19}$ [8]. The relation between size and shape of the coordination polyhedron and the energy of the $4f^{n-1}5d^1$ crystal-field states of trivalent rare-earth ions was recently discussed by Dorenbos in a series of publications [17–19]. From this work and the fact that the shapes and sizes of the coordination polyhedra around Sr^{2+} and La^{3+} in $Sr_{0.7}La_{0.3}Al_{11.7}Mg_{0.3}O_{19}$ are identical to those for Sr^{2+} in $SrAl_{12}O_{19}$, PCE is expected in $Sr_{0.7}La_{0.3}Al_{11.7}Mg_{0.3}O_{19}$.

2. Experimental procedures

2.1. Synthesis

The growth of $SrAl_{12}O_{19}$ is non-congruent and the parasitic phases α-Al_2O_3, $SrAl_2O_4$, and $SrAl_4O_7$ are formed from the melt. In order to avoid the formation of these phases, $Sr_{1-x}La_xMg_yAl_{12-y}O_{19}$ single crystals were grown with $x = y = 0.3$. This compound does melt congruently and crystals were grown by the Czochralski method in iridium crucibles under an argon atmosphere with a pulling rate of 0.5 mm h^{-1} and a rotation of the seed of 25 rotations min^{-1}. The crystals obtained (20 mm in diameter, 50 mm long) present a spontaneous growth along the *c*-direction and have good optical quality [20, 21].

The crystal structure of $Sr_{1-x}La_xMg_yAl_{12-y}O_{19}$ is identical to that of $SrAl_{12}O_{19}$ and is of the magnetoplumbite type with space group P_{63}/mmc (No 193) [22]. Sr and La ions are randomly distributed over the available sites in the intermediate layer. They are twelvefold coordinated in the form of a cuboctahedron of oxygen ions at an average distance (R_{av}) of 279.1 pm with point symmetry D_{3h}. The final concentration of the crystal studied ($10 \times 10 \times 1$ mm) obtained by ion-coupled plasma (ICP) measurements of a 5% Pr^{3+} starting composition was $Sr_{0.646}La_{0.281}Pr_{0.035}Mg_{0.332}Al_{11.658}O_{19}$. The lower Pr^{3+} concentration in the crystal compared to the melt is due to the distribution coefficient being smaller than one. The molten part enriched its Pr^{3+} concentration during the crystal growth process. The molecular formula of the crystal studied will be denoted as $Sr_{0.7}La_{0.3}Al_{11.7}Mg_{0.3}O_{19}$:3.5% Pr^{3+}.

The method of preparation of the SrB_4O_7:1% Pr^{3+} sample involved forming a mixture of strontium carbonate and praseodymium oxide in an aqueous solution of boric acid at 80 °C. The mixture was dried at 90 °C to form a solid precipitate. The resulting product was fired for 7–10 h at 950 °C in a 5% H_2/95% N_2 flow. The sample was checked by x-ray diffraction (XRD) using Cu Kα radiation. No impurity phases were detected in the XRD pattern.

SrB_4O_7 has the space group $P21/nm$ (No 31) and belongs to the triclinic crystal system. There is one crystallographic Sr site available for Pr^{3+} that has a ninefold coordination with an R_{av} of 269.5 pm and a C_i point symmetry [23].

2.2. Measurements

Room temperature emission and excitation spectra in the 200–800 nm wavelength range were performed with a spectrophotometer with a Xe lamp. Its characteristics were described before [24]. Low-temperature excitation and emission spectra were taken using liquid helium at Deutsche Electronen Synchrotron (DESY) in Hamburg (Germany) using the SUPERLUMI station of Hasylab. Details of this excitation facility have been described elsewhere [25]. The spectral region of excitation was 50–300 nm with a fixed resolution of 0.3 nm. Luminescence could be detected either in the 150–300 nm region utilizing a solar-blind PMT or in the

200–600 nm region using a cooled R2059 PMT. The maximal obtainable resolution of both emission branches was 1 nm. The synchrotron operated in multibunch mode with bunches separated by 200 ns. X-ray-excited emission spectra between 200 and 550 nm were obtained using an ARC VM504 vacuum monochromator (see reference [24]). Between 550 and 800 nm a Peltier-cooled R943-02 Hamamatsu PMT was used in addition to an EMI PMT, used between 200 and 550 nm. The x-ray-excited emission spectra were not corrected for wavelength-dependent detection efficiency. For the other emission spectra the best available correction curves were used. Still, relative emission intensities should be interpreted with care. Excitation spectra were corrected for the wavelength-dependent excitation intensity using sodium salicylate as a reference material.

3. Results and discussion

3.1. $Sr_{0.7}La_{0.3}Al_{11.7}Mg_{0.3}O_{19}$:3.5% Pr^{3+}

3.1.1. 10 K excitation and emission measurements. Figure 2(a) displays the time-integrated emission spectrum between 200 and 300 nm of $Sr_{0.7}La_{0.3}Al_{11.7}Mg_{0.3}O_{19}$, recorded at 12 K and 190 nm pulsed excitation. The three strongest lines at 216.0, 253.3, and 273.5 nm are the transitions from the $^1S_0$ state to the $^3H_4$, $^3F_4$, and $^1G_4$ sates respectively. Lines of lower intensity, corresponding to the $^3F_2$ and $^3H_6$ states, are found at 239.3 and 242.7 nm. Between 220 and 290 nm, broad-band emission is observed.

When the emission is recorded under the same experimental conditions but collecting light between 2 and 10 ns (figure 2(b)), broad bands peaking at 240 and 265 nm appear more prominent relative to $^1S_0$ emission. They are assigned to 4f5d $\rightarrow$ 4f^2[^{3}H, ^{3}F] emission (d $\rightarrow$ f emission) because of their spectral shape and energy which are typical for d $\rightarrow$ f emission of Pr^{3+} and because of the fast ns decay.

In a time window from 125 to 190 ns (figure 2(c)), $^1S_0 \rightarrow {}^3H_6$ and $^1S_0 \rightarrow {}^3F_2$ transitions are observed more clearly relative to the faster d $\rightarrow$ f emission, and the $^1S_0 \rightarrow {}^3H_5$ transition can be observed at 226.5 nm while the transition to the $^3F_3$ state is not detected. Since the $^1S_0$ emission has a decay time of about 700 ns [26], 10–30 times longer than that of the d $\rightarrow$ f decay time, a proportion of the $^1S_0$ emission in figures 2(b) and 2(c) originates from the accumulated effect of several preceding excitation pulses.

In figure 3(a) the time-integrated excitation spectrum, recorded at 12 K, is plotted, monitoring 273.5 nm emission. At this wavelength both $^1S_0 \rightarrow {}^1G_4$ emission and d $\rightarrow$ f emission are observed. The narrow line at 215.3 nm is assigned to $^3H_4 \rightarrow {}^1S_0$ excitation and is superimposed on weak broad bands. The most intense broad excitation bands with maxima at 187, 192, and 197 nm are assigned to 4f^2[^{3}H$_4$] $\rightarrow$ 4f5d excitation. The excitation intensity drops towards shorter wavelengths, with a local maximum at 174 nm, until 145 nm is reached, where the intensity diminishes. A faint shoulder is observed at about 185 nm.

In the excitation spectrum, recorded at 12 K, monitoring the 4f5d $\rightarrow$ 4f^2 emission at 240 nm, excitation bands are observed at 219 and 204 nm (figure 3(b)). Three local minima are found at 215, 197, and 192 nm, i.e. at the same wavelengths as the maxima of the $^1S_0$ and 4f5d states as measured in figure 3(a) when monitoring the 273 nm emission. At shorter wavelengths the excitation spectrum has an identical shape to that in figure 3(a).

Apparently there are two types of Pr^{3+} ion present: one with the lowest-energy excited state of the 4f5d configuration above the $^1S_0$ state yielding $^1S_0$ emission (site Pr_I) and a site with that state below the $^1S_0$ state yielding 4f5d $\rightarrow$ 4f^2 emission (site Pr_{II}). The local minima in the excitation spectrum of d $\rightarrow$ f emission of Pr_{II} is attributed to competing absorption by Pr_I. If the spectrum in figure 3(b) is scaled to that of figure 3(a) (at 218 nm) and subsequently

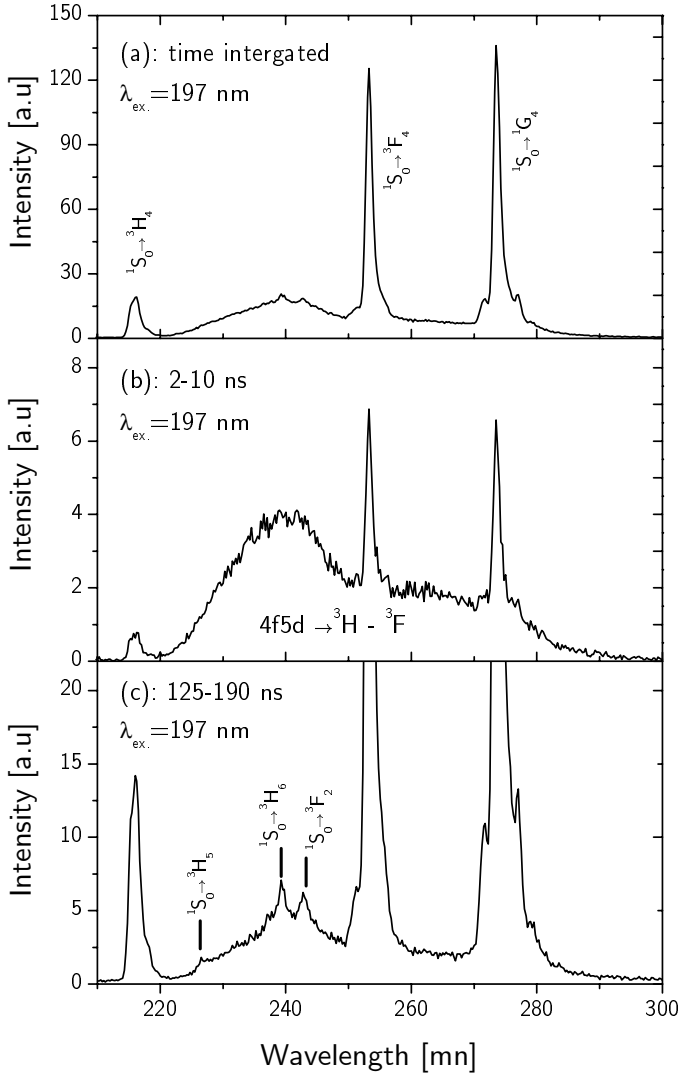

Figure 2. The emission spectrum of $Sr_{0.7}La_{0.3}Al_{11.7}Mg_{0.3}O_{19}$:3.5% Pr^{3+}, recorded at liquid-He temperature at 190 nm pulsed excitation for different time windows: (a) time integrated; (b) 2–20 ns; (c) 25–160 ns.

subtracted from it, one obtains the spectrum plotted in figure 3(c). It represents the excitation spectrum of Pr_I luminescence. The $^1S_0$ state is now observed clearly isolated from the onset of the 4f5d configuration at 215.3 nm (46 450 cm^{-1}).

3.1.2. Room temperature emission. The most intense emission lines observed at 445 nm excitation (figure 4, curve (a)) are assigned to $^3P_0$ emission to the various ^3F and ^3H states as indicated in the figure. We do not think that emission lines originating from the $^1D_2$ level are present since $^3P_0 \rightarrow {}^1D_2$ multiphonon relaxation is inefficient in this lattice due to the low phonon energies of about 650 cm^{-1}, typical for aluminates, with respect to the $^3P_0 \rightarrow {}^1D_2$ energy gap. Also $^1D_2$ luminescence is often efficiently quenched at concentrations above

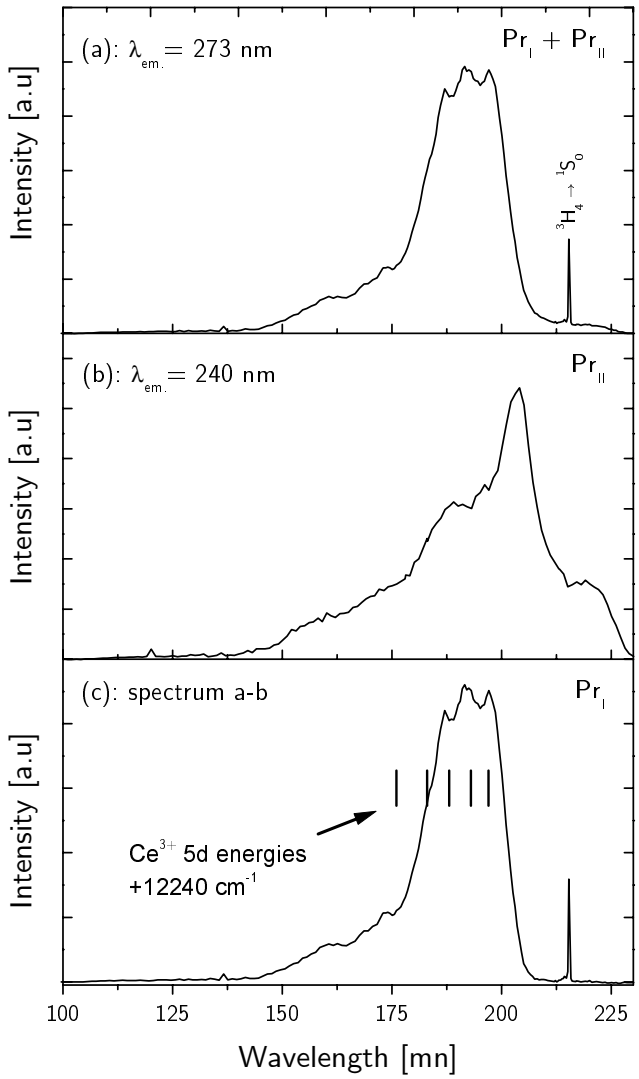

Figure 3. Excitation spectra of $Sr_{0.7}La_{0.3}Al_{11.7}Mg_{0.3}O_{19}$:3.5% Pr^{3+} recorded at liquid-He temperature, monitoring (a) 273 nm and (b) 240 nm emission. Spectrum (c) is obtained by subtracting spectrum (b) from (a).

1% Pr^{3+}. In the same figure the excitation spectrum is plotted, monitoring the $^3P_0 \rightarrow {}^3H_6$ emission at 624 nm. Excitation lines (curve (b)) are assigned to the $^3P_0$, $^3P_1$, and $^3P_2$ states.

Under 220 nm excitation (figure 5) Pr_{II} ions are excited exclusively and 4f5d $\rightarrow$ $4f^2[^3H, {}^3F]$ emission is observed with the most intense bands peaking at 245 and 280 nm. The $^3P_0$ emission after 4f5d excitation is often observed simultaneously with d $\rightarrow$ f emission and is explained by a non-radiative 4f5d $\rightarrow$ $4f^2[^3P, {}^6I]$ relaxation feeding the $^3P_0$ state.

At 200 nm excitation (figure 6(a)) both Pr_I and Pr_{II} are excited efficiently according to the excitation spectra of figures 3(b) and 3(c), but the emission is predominantly from Pr_I, i.e., $^1S_0$ emission followed by $^3P_0$ emission. This is in accordance with the PCE process and in agreement with the Pr^{3+} luminescence in $SrAl_{12}O_{19}$ [8]. Only weak d $\rightarrow$ f emission is

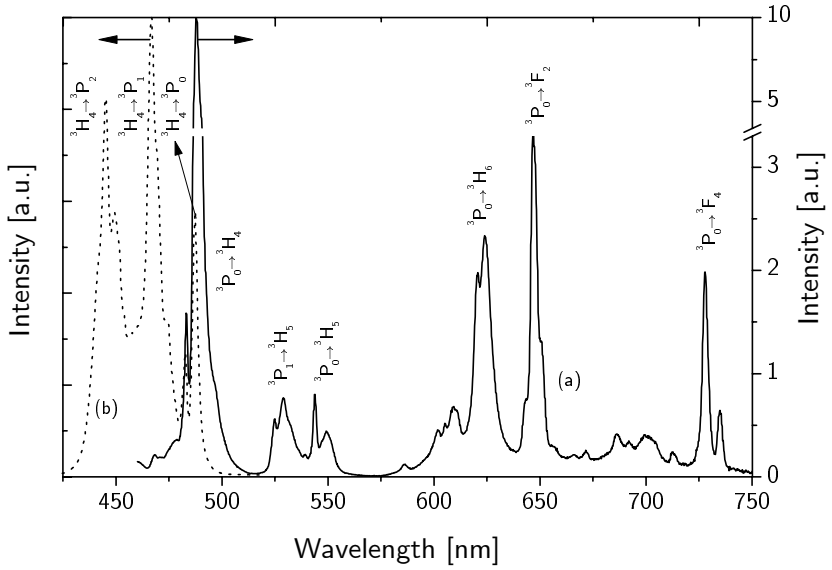

Figure 4. (a) The excitation spectrum of $Sr_{0.7}La_{0.3}Al_{11.7}Mg_{0.3}O_{19}$:3.5% Pr^{3+} recorded at room temperature for the $^3P_0 \rightarrow {}^3H_6$ emission and (b) the emission spectrum at 445 nm excitation.

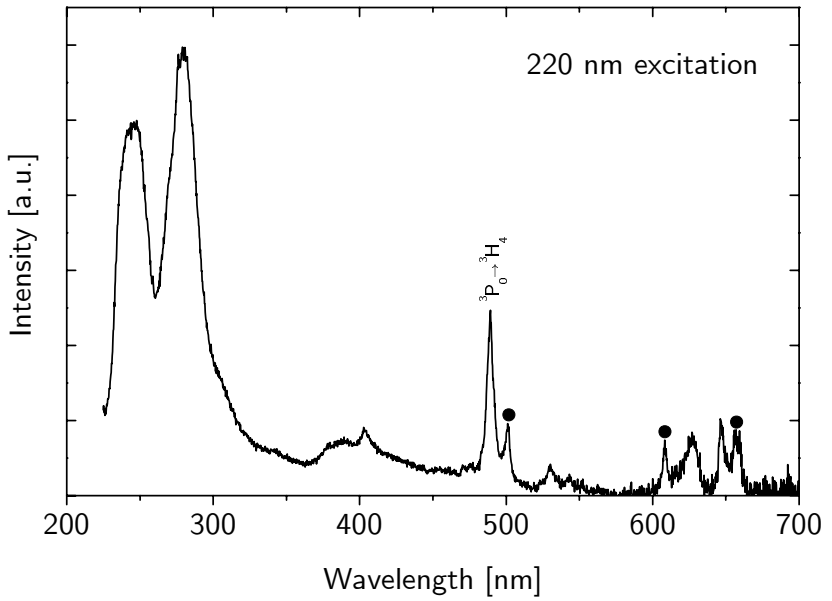

Figure 5. The emission spectrum of $Sr_{0.7}La_{0.3}Al_{11.7}Mg_{0.3}O_{19}$:3.5% Pr^{3+} recorded at room temperature at 220 nm excitation.

observed from which it is concluded that Pr_I is much more abundant than Pr_{II}. The intensity ratio of the $^1S_0 \rightarrow {}^1I_6$ and the total $^3P_0$ emission is 1:4, from which the total quantum efficiency of the $^3P_0$ emission can be estimated to be 25%. 75% of the Pr^{3+} ions decay non-radiatively, most probably by concentration quenching, which is not unusual at a concentration of 3.5%.

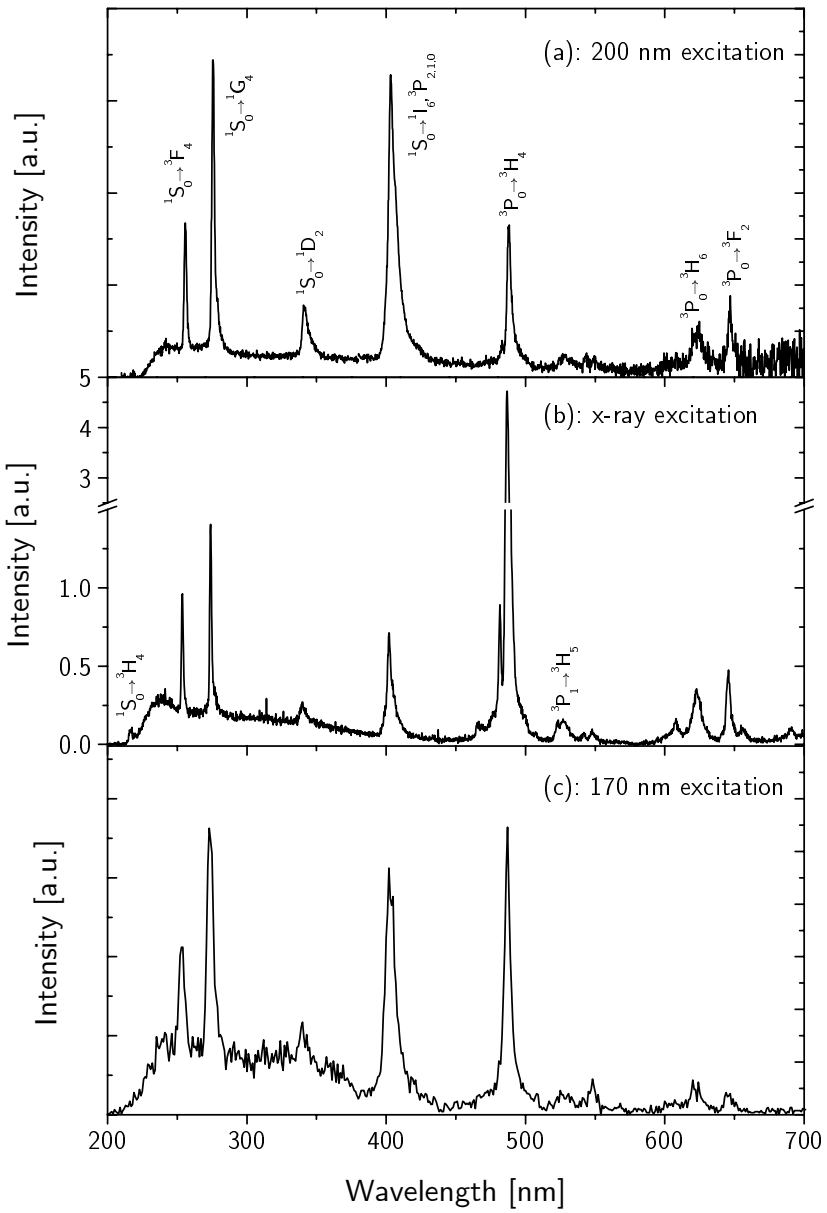

Figure 6. The emission spectrum of $Sr_{0.7}La_{0.3}Al_{11.7}Mg_{0.3}O_{19}$:3.5% Pr^{3+} recorded at room temperature at: (a) 200 nm; (b) x-ray; and (c) 170 nm excitation.

The visible $^3P_0$ emission from Pr_I can be distinguished from that of Pr_{II}. Three emission lines, marked by the black dots in figure 5, are only observed when Pr_{II} ions are excited selectively at 220 nm; they are absent in figure 6(a).

The nature of the weak broad background that is observed between 275 and 500 nm, partly overlapping the $4f5d \rightarrow 4f^2$ emission, is unclear. We do not believe that it is due to $4f5d \rightarrow 4f^2$ emission since such an emission is usually limited to the UV. Because this emission is observed at excitation energies lower than the band-gap energy, it cannot be of excitonic

nature. Charge-transfer transitions involving Pr^{3+} are also not expected. The most likely assignment is emission from defect centres induced by VUV and x-ray excitation of preceding experiments. Prolonged x-ray excitation resulted in a brown coloration of the crystal. The broad emission as observed in figure 2(b) drops to zero at 300 nm. Such a drop is not observed in the emission plotted in figure 6(a). The latter spectrum was however recorded after VUV and x-ray excitation experiments. The broad emission in figure 6(a) may therefore originate from defect centres that were not present at the moment when the spectra of figure 2(b) were recorded.

Spectral lines in the x-ray-excited emission spectrum (figure 6(b)), recorded at room temperature, are assigned to emission from the $^1S_0$ state and the $^3P_0$ state as discussed before. The total $^3P_0$ emission intensity relative to the $^1S_0 \rightarrow {}^1I_6$, $^3P_{2,1,0}$ emission intensity is about 20 times higher than could have been expected according to the PCE process assuming a QE of 25% of the total $^3P_0$ emission. Apparently the $^3P_0$ state is excited directly and not via the $^1S_0 \rightarrow {}^1I_6$, $^3P_{2,1,0}$ transition. The difference in intensity ratio between 200 nm and x-ray excitation can be explained by assuming that 95% of the Pr^{3+} ions are excited directly in the $^3P_0$ state without $^1S_0 \rightarrow {}^1I_6$, $^3P_{2,1,0}$ transfer and only 5% of the Pr^{3+} ions are excited via the $^1S_0$ state.

Finally, at 170 nm (PDP) excitation (figure 6(c)), we find that the ratio of the $^1S_0 \rightarrow {}^1I_6$, $^3P_{2,1,0}$ and the total $^3P_0$ emission is about 1:1. This value will be discussed later.

3.2. SrB_4O_7:1% Pr^{3+}

The emission spectrum of SrB_4O_7:1% Pr^{3+} recorded at 12 K and at 188.5 nm excitation is plotted in figure 7. Groups of emission lines are found at 216, 225, 237, 242, 253, (271, 273), 340, and (396, 403) nm, and assigned respectively to transitions from the $^1S_0$ state to the

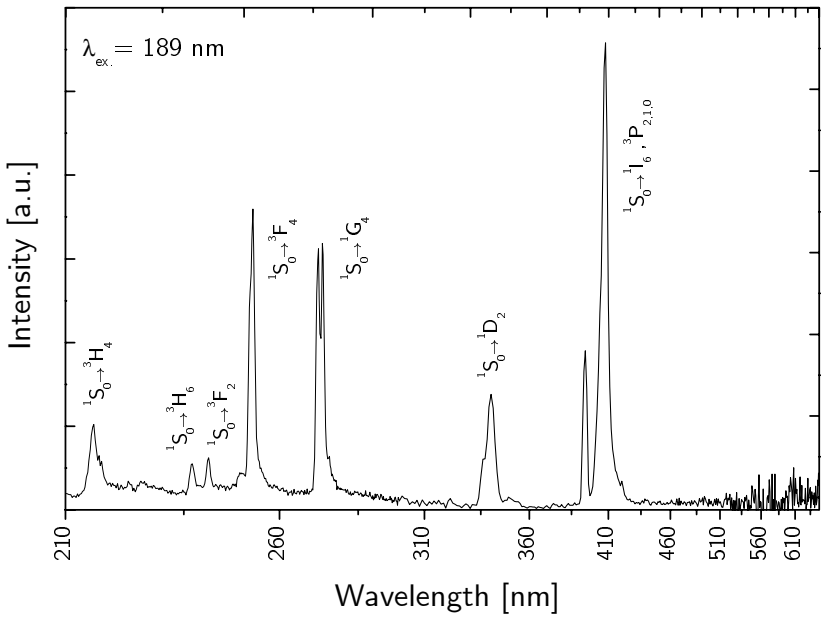

Figure 7. The time-integrated emission spectrum of SrB_4O_7:1% Pr^{3+} recorded at liquid-He temperature at 189 nm pulsed excitation.

Stark levels of the $^3H_4$, $^3H_5$, $^3H_6$, $^3F_2$, $^3F_4$, $^1G_4$, $^1D_2$, and $^1I_6$, $^3P_{2,1,0}$ multiplets of the $4f^2$ configuration of Pr^{3+}. As can be seen in figure 7, no emission from the $^3P_0$ state is observed although this was expected on the basis of the PCE process.

In the excitation spectrum, recorded at 12 K, monitoring the $^1S_0 \rightarrow {}^1I_6, {}^3P_{2,1,0}$ emission at 409 nm (figure 8), two bands are present at 190 and 210 nm due to $4f^2 \rightarrow 4f5d$ excitation, both having additional structure. The bands between 125 and 165 nm correspond to host lattice excitation [27, 28]. $^3H_4 \rightarrow {}^1S_0$ excitation is expected around 214 nm, which is below the onset of the $4f \rightarrow 5d$ excitation band observed at 212 nm. Still, the corresponding excitation line was not detected, not even in a separate experiment with better signal-to-noise ratio and smaller step size (0.1 nm instead of 1 nm) of the excitation monochromator (see the inset in figure 8).

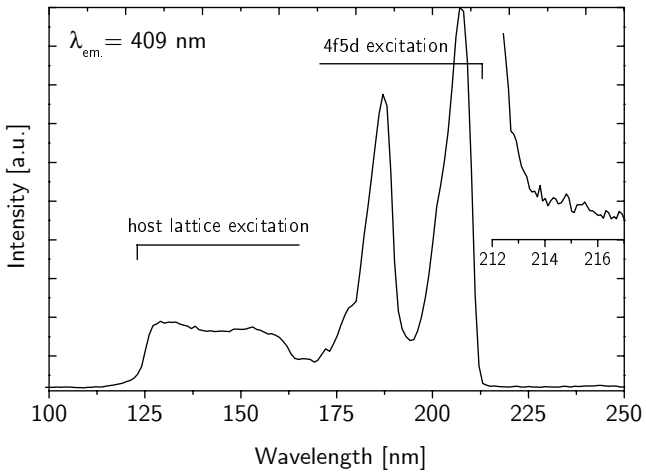

Figure 8. The excitation spectrum of SrB_4O_7:1% Pr^{3+}, recorded at liquid-He temperature, monitoring 409 nm emission ($^1S_0 \longrightarrow {}^1I_6, {}^3P_{2,1,0}$).

The emission spectrum recorded at room temperature and at 444 nm excitation ($^3P_2$ state) displays no emission from the $^3P_0$ state but weak $^1D_2 \rightarrow {}^3H_4$ emission around 600 nm (figure 9, curve (a)). The excitation spectrum of this emission (figure 9, curve (b)) shows the ^3P_J, $^1I_6$ excited states. Both spectra demonstrate that the $^1D_2$ level is fed efficiently via the $^3P_0$ level non-radiatively.

4. Discussion

4.1. $Sr_{0.7}La_{0.3}Al_{11.7}Mg_{0.3}O_{19}$:3.5% Pr^{3+}

The excitation and emission spectra of $SrAl_{12}O_{19}$:Pr^{3+} were measured by Srivastava and Beers [8]. The maximum of the 4f5d configuration was observed at approximately 195 nm which agrees with our observations. The excitation spectrum of Ce^{3+} in $SrAl_{12}O_{19}$ was measured by Verstegen [29] and Stevels [30]. Crystal-field states of the 5d configuration of Ce^{3+} were observed in these works at 224, 235, 244, 252, and 261 nm. A constant energy difference of 12 240 cm^{-1}, between the lowest-energy crystal-field state of Ce^{3+} and the lowest-energy state of the 4f5d configuration of Pr^{3+}, can be added to all of the crystal-field states of Ce^{3+}, merely to get an indication of the total width and energy of the 4f5d configuration of Pr^{3+} in $Sr_{0.7}La_{0.3}Al_{11.7}Mg_{0.3}O_{19}$. The wavelengths that are calculated in this way are 197, 193, 188, 183, and 176 nm and are in reasonable agreement with the maxima as observed in spectrum 3(c).

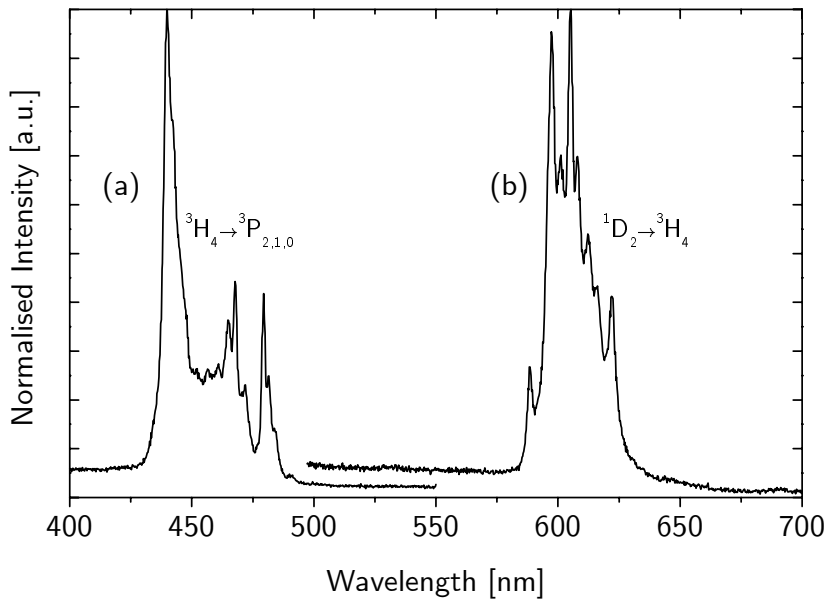

Figure 9. (a) The excitation spectrum of SrB_4O_7:1% Pr^{3+}, recorded at room temperature, monitoring 600 nm emission ($^1D_2 \longrightarrow {}^3H_4$). (b) The emission spectrum of SrB_4O_7:Pr^{3+}, recorded at room temperature at 444 nm ($^3P_2$) excitation.

By comparing the excitation spectra of Ce^{3+} and Pr^{3+} it is concluded that the excitation bands between 145 nm and ≈175 nm in figure 3(c) originate from host lattice excitation. This is in agreement with findings for other hexa-aluminates in which a host lattice absorption onset at about 185 nm and a maximum at 170 nm were observed [28,31]. The host lattice absorption partly overlaps with the 4f5d configuration that is observed roughly between 180 and 200 nm.

The presence of a second less abundant site (Pr_{II}) with d → f emission was not observed in $SrAl_{12}O_{19}$. Also here Mg^{2+} was used as a charge-compensating ion. When Pr^{3+} replaces Sr^{2+} in $SrAl_{12}O_{19}$ or $Sr_{0.7}La_{0.3}Al_{11.7}Mg_{0.3}O_{19}$, charge compensation is achieved by the substitution of equal amounts of Mg^{2+} for Al^{3+} in the middle of the spinel blocks of the magnetoplumbite structure. This means that charge compensation does not change the coordination sphere around Pr^{3+} in the intermediate layer and therefore cannot explain the presence of the two sites for Pr^{3+}. It is interesting to note that $SrAl_{12}O_{19}$ and $LaMgAl_{11}O_{19}$ have the same crystal structure, with identical anion coordination shapes around the large metal ion. The size of the coordination sphere is however slightly smaller in the case of $LaMgAl_{11}O_{19}$ and the Pr^{3+} luminescence in $LaMgAl_{11}O_{19}$ is of the Pr_{II} type. One might therefore identify the Pr_{II} site with Pr ions on a site similar to that in $LaMgAl_{11}O_{19}$. However, the f → d energy difference between Pr_I and Pr_{II} (see figure 3) of 5100 cm^{-1} is considerably larger than the Ce^{3+} f → d energy difference of 1250 cm^{-1} between $LaMgAl_{11}O_{19}$ and $SrAl_{12}O_{19}$. We think that it is more likely that the Pr_I and Pr_{II} sites possess different anion coordination shapes, resulting in a larger crystal-field splitting.

In this respect we note that in both $LaMgAl_{11}O_{19}$ and $SrAl_{12}O_{19}$ two Ce^{3+} sites have been observed [30]: one regular site with UV emission and one so-called Ce–O associate site with blue emission. The latter site is believed to be a Ce^{3+} ion with one nearby oxygen ion that is pushed towards Ce^{3+} by a second oxygen ion that replaces a La or Sr ion in the intermediate layer. The f → d energy difference between these two Ce^{3+} sites in $LaMgAl_{11}O_{19}$ is about

5000 cm^{-1} [30], a value similar to the f $\rightarrow$ d energy difference between Pr_I and Pr_{II} in $Sr_{0.7}La_{0.3}Al_{11.7}Mg_{0.3}O_{19}$.

The high intensity of $^3P_0$ emission relative to $^1S_0$ emission as observed in figure 4(b) is explained as follows. Thermalized electron–hole pairs created upon x-ray excitation have a high probability of exciting the abundant Pr_I ions either by direct trapping of the electrons and the holes (process I), or via the formation of a self-trapped-exciton-like state that can transfer its energy to a Pr ion (process II). These two processes are schematically indicated in figure 10. Similar types of mechanism are thought to occur in Ce^{3+}-doped scintillator materials [24, 32–34].

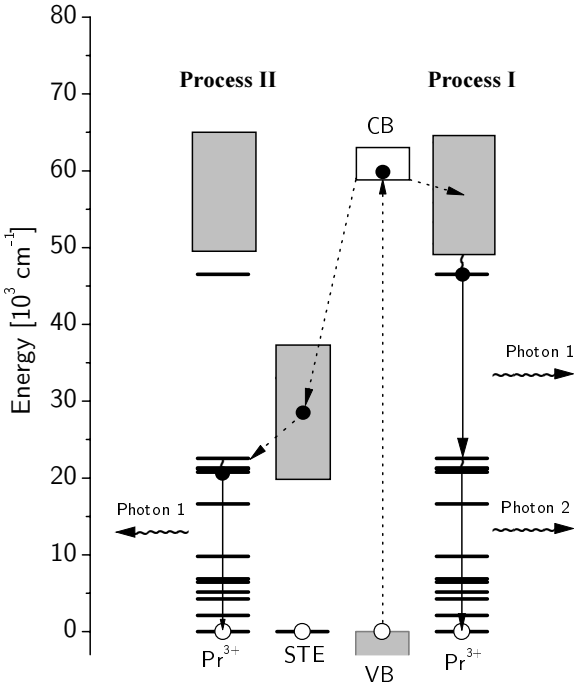

Figure 10. A schematic representation of direct electron–hole pair recombination involving the 4f5d states leading to Pr^{3+} $^1S_0$ excitation (process I) and Pr^{3+} $^3P_0$ excitation via an intermediate STE state (process II).

Self-trapped-exciton (STE) emission in $Sr_{0.7}La_{0.3}Al_{11.7}Mg_{0.3}O_{19}$ is not observed at room temperature and no attempts were made to measure the STE emission at low temperature. We believe however that the $^1S_0$ emission at x-ray excitation is most probably due to process I. The 4f5d states partly overlap with the conduction band states and electrons can be captured by Pr^{3+} ions directly from the conduction band into the 4f5d states followed by emission from the $^1S_0$ state. Process I cannot result in $^3P_0$ emission without preceding $^1S_0$ emission. Therefore we believe that the $^3P_0$ state is mainly excited via process II. Apparently the STE emission does not overlap with the high-energy $^1S_0$ state but does overlap with the lower-energy ^3P_J or $^1I_6$ states.

A similar behaviour at x-ray excitation to that observed in $Sr_{0.7}La_{0.3}Al_{11.7}Mg_{0.3}O_{19}$ was observed before in LaF_3 [35] and discussed by Srivastava and Duclos [36]. It was argued that the recombination energy of the STE may be resonant with the $^1S_0$ state resulting in the PCE process as observed in YF_3 [36] or with the $^3P_{2,1,0}$ and $^1I_6$ states resulting in $^3P_0$ emission as

observed in LaF_3 [35]. Recently, Van der Kolk *et al* [16] observed that the overlap between the STE emission and $^3H_4 \rightarrow {}^1S_0$ excitation plays a role in the energy transfer from the host lattice to Pr^{3+} in $BaSiF_6$:Pr^{3+}.

The role of STEs, involving energy transfer from the host lattice to the Pr^{3+} in $SrLa_{0.3}Al_{11.7}Mg_{0.3}O_{19}$:$Pr^{3+}$, is identical to that observed in several Ce^{3+}-doped scintillators. STE $\rightarrow Ce^{3+}$ energy transfer was recently studied as a function of activator concentration and temperature by van 't Spijker and co-workers in K_2LaCl_5 and $BaLu_2F_8$ [33, 37] and in $LaCl_3$ by Guillot-Noël *et al* [24].

The larger amount of $^3P_0$ emission relative to $^1S_0 \rightarrow {}^1I_6$ emission at 170 nm excitation, compared to 200 nm excitation, can be understood if it is assumed that the same excitons are created at host lattice excitation (170 nm) and x-ray excitation. From the observed ratio of 1:1 (figure 6(b)), the quantum efficiency of the $^3P_0$ state (25%), and the observation that 95% of host lattice excitation results in $^3P_0$ emission, we can conclude that 40% of 170 nm radiation is absorbed by Pr^{3+} and 60% by the host lattice. It must be noted that this is an unfavourable situation as regards the possibility of applying $SrLa_{0.3}Al_{11.7}Mg_{0.3}O_{19}$:$Pr^{3+}$ as a quantum splitting phosphor in PDPs or Xe/Ne-filled lighting tubes where phosphors are excited mainly at 170 nm.

It is not possible to draw definite conclusions about the formation and nature of the self-trapped exciton in $SrLa_{0.3}Al_{11.7}Mg_{0.3}O_{19}$ on the basis of our measurements. One might suggest, in analogy with the formation of a STE in alkali halides (see for example reference [38]), that first a hole is trapped by two O^{2-} anions after which a V_K centre is formed. Subsequently the electron is trapped by the V_K centre via the conduction band, forming the STE.

The energy transfer from the host lattice to the $^3P_0$ state can also explain the sharp drop in intensity of the 4f5d excitation spectrum at 180 nm and shorter wavelengths seen when monitoring the $^1S_0$ emission (figure 3). It is due to a competing absorption between the host lattice and the 4f5d excited states of Pr^{3+}.

4.2. SrB_4O_7:1% Pr^{3+}

The emission characteristics of Pr^{3+} in SrB_4O_7 were described before by Verwey *et al* [15]. In that work emission lines were observed at 217, 225, 241, 252, and 272 nm on top of broad-band emission and were incorrectly assigned to parity-allowed 4f5d $\rightarrow 4f^2$ transitions. The emission of Pr^{3+} in SrB_4O_7 closely resembles that of Pr^{3+} in $LaMgB_5O_{10}$ [9] and LaB_3O_6 [10]. Also in these hosts $^1S_0 \rightarrow {}^1I_6$ emission was observed while no emission from the $^3P_0$ state, which is expected according to the PCE process, could be detected. This was explained by an efficient $^3P_0 \rightarrow {}^1D_2$ multiphonon relaxation due to the high (1400 cm^{-1}) phonon energies of the borate host lattice compared to the energy gap between the $^3P_0$ and $^1D_2$ levels (3400 cm^{-1}). The same arguments can be adopted to explain the absence of $^3P_0$ luminescence in SrB_4O_7. The poor efficiency of the $^1D_2$ luminescence was however not discussed in references [9] and [10]. The $^3P_0 \rightarrow {}^1D_2$ multiphonon relaxation excites the $^1D_2$ level and should intensify the luminescence from that level. $^1D_2 \rightarrow {}^1G_4$ multiphonon relaxation is less efficient because of the larger energy gap of 6500 cm^{-1} between these levels. Using the modified energy gap law of van Dijk and Schuurmans [39] with the constants β_{el} and α as in references [9] and [10], the non-radiative multiphonon rate, involving five phonons, is calculated to be about 100 times lower than the typical radiative rate of the $^1D_2$ level of about 2000 s^{-1} ($\tau \approx 500\ \mu s$) [40]. The poor efficiency of the $^1D_2$ emission is therefore more probably due to cross-relaxation involving nearest-neighbour Pr^{3+} ions. It is well known that cross-relaxation paths exist between two Pr^{3+} ions such as $^1D_2(Pr_1) + {}^3H_4(Pr_2) \rightarrow {}^3F_4(Pr_1) + {}^1G_4(Pr_2)$ and that they can completely quench the $^1D_2$ luminescence even at a 1% Pr^{3+} concentration [41–43]. A detailed experimental study

to reveal the exact quenching process in this host lattice is beyond the scope of this work. It remains to be investigated to what extent the $^1D_2$ emission intensity is actually recovered at lower Pr^{3+} concentrations. Perhaps Pr^{3+} ions are incorporated preferentially as pairs in the SrB_4O_7 hosts or maybe the multiphonon relaxation process is more efficient than what is calculated using the energy gap law due to the high phonon energy and large energy gap.

The lowest-energy 4f5d state of Pr^{3+} in SrB_4O_7 is observed 1100 cm^{-1} above the $^1S_0$ state. Such a high-energy 4f5d state results in PCE and was also observed in $LaMgB_5O_{10}$ and LaB_3O_6. It was explained by a high coordination number (CN) and large average Pr^{3+}–O^{2-} distances R_{av} (CN = 9, R_{av} = 257.2 pm in $LaMgB_5O_{10}$ [44] and CN = 10, R_{av} = 261.2 pm in LaB_3O_6 [45]). Such a Pr^{3+} coordination results in a weak crystal field and in a small crystal-field splitting of the 4f5d configuration. As a consequence the lowest-energy 4f5d state will be at a higher energy than the $^1S_0$ state. A minimum R_{av} of 256.1 pm was claimed for oxides in patents [46, 47], above which $^1S_0$ emission and the corresponding PCE process can be expected. There are however many oxides that have a higher CN and larger R_{av} and low-energy 5d states. For example $LaAlO_3$ (CN = 12 and R_{av} = 267.9 pm) and $SrTiO_3$ (CN = 12 and R_{av} = 275.8 pm) both have the lowest-energy 4f5d state at a much lower energy compared to the borates and much lower than is expected on the basis of anion coordination alone. The high-energy 4f5d states of the borates originate not only from the small crystal-field splitting but also from a high-energy centroid (the average energy of the 4f5d states). It was already noted by Blasse [48] and Fouassier *et al* [49] and recently further investigated by Dorenbos [17, 18] that small and highly charged cations next to the large cation that is to be replaced by the rare-earth ion raise the centroid energy of the $4f^{n-1}5d^1$ states. Furthermore, borates are found in condensed forms (chains or planes of corner-sharing $(BO_3)^{3-}$ triangles) that increase the number of B^{3+} ions relative to the number of O^{2-} ions. It was shown by Dorenbos [50] that a high degree of condensation between ionic $(BO_3)^{3-}$ complexes promotes a high-energy centroid, not only in borates but also in phosphates. The high energy of the first 4f5d transitions in the condensed borates $LaMgB_5O_{10}$, LaB_3O_6, and also SrB_4O_7 is due to the high centroid energy as well as the small crystal-field splitting of the 4f5d states.

The excitation spectrum of the $^1S_0$ emission as observed in figure 8 consists of 4f5d excitation bands and less intense bands due to host lattice excitation. The absorption efficiency of the host lattice compared to the absorption efficiency of the 4f5d states of Pr^{3+} is expected to be higher since Pr^{3+} is doped into the host at a concentration of 1%. This implies that the energy transfer from the borate host lattice to the Pr^{3+} $^1S_0$ state is very inefficient. When this energy transfer is efficient, which is for example the case for commercially available PDP phosphors like $Ba_{0.75}Al_{11}O_{17.25}$:$Mn^{2+}$, $(Y, Gd)_2O_3$:Eu^{3+}, $BaMgAl_{11}O_{19}$:Eu^{2+}, the host lattice excitation bands are as intense as the excitation bands related to the activators.

5. Conclusions

Emission from the $^1S_0$ state is observed in $SrLa_{0.3}Al_{11.7}Mg_{0.3}O_{19}$ and SrB_4O_7 at 4f5d excitation. In $SrLa_{0.3}Al_{11.7}Mg_{0.3}O_{19}$ the $^1S_0 \rightarrow {}^1I_6$, $^3P_{2,1,0}$ emission is followed by $^3P_0$ emission that has a quantum efficiency of 25%. In SrB_4O_7 the $^3P_0$ emission is quenched by multiphonon relaxation and only weak $^1D_2$ emission is observed instead. The lowest-energy 4f5d states are observed at 197 and 210 nm for the aluminate and the borate respectively. These values could be predicted prior to measurement on the basis of the Ce^{3+} excitation properties in these hosts. Both phosphors are unsuited for application in a PDP or Xe-filled TL because the largest part of the excitation energy in the VUV is absorbed by the host lattice and is not transferred efficiently to the $^1S_0$ state of Pr^{3+}. In the aluminate, the energy transfer from the host is preferentially to the $^3P_0$ state instead of the desired $^1S_0$ state.

Acknowledgments

We gratefully acknowledge B Viana from the LCAES-ENSCP Laboratory of Paris for providing the $SrLa_{0.3}Al_{11.7}Mg_{0.3}O_{19}$ crystal and we thank I Berezovskaya and V Dotsenko of the A V Bogatsky Physico-Chemical Institute (Odessa, Ukraine) for the synthesis of the SrB_4O_7 sample. The authors wish to thank HASYLAB for beamtime at the SUPERLUMI experimental station. These investigations were supported by the Netherlands Technology Foundation (STW). Human mobility was supported by the European Commission and the Van Gogh programme of the Netherlands Organization for Scientific Research (NWO).

References

[1] Kamegaya T, Matsuzaki H and Yokozawa M 1978 *IEEE Trans. Electron. Devices* **25** 1094–100
[2] Sommerdijk J L, Bril A and de Jager A W 1974 *J. Lumin.* **8** 288–96
[3] Sommerdijk J L, Bril A and de Jager A W 1974 *J. Lumin.* **8** 341–3
[4] Piper W W, DeLuca J A and Ham F S 1974 *J. Lumin.* **8** 344–8
[5] Wegh R T, Donker H, van Loef E V D, Oskam K D and Meijerink A 2000 *J. Lumin.* **87+89** 1017–19
[6] Wegh R T, van Loef E V D and Meijerink A 2000 *J. Lumin.* **90** 111–22
[7] Jüstel T, Nikol H and Ronda C 1998 *Angew. Chem. Int. Ed.* **37** 3084–103
[8] Srivastava A M and Beers W W 1997 *J. Lumin.* **71** 285–90
[9] Srivastava A M, Doughty D A and Beers W W 1996 *J. Electrochem. Soc.* **143** 4113–6
[10] Srivastava A M, Doughty D A and Beers W W 1997 *J. Electrochem. Soc.* **144** L190–2
[11] Bayer E, Leppert J, Grabmaier B C and Blasse G 1995 *Appl. Phys.* A **61** 177–81
[12] Ramesh Babu V, Rama Moorthy L and Buddhudu S 1986 *Acta Cienc. Indica* **12** 69–71
[13] van der Kolk E, Dorenbos P, Vink A P, van Eijk C W E, Perego R C and Lakshmanan A R 2001 to be submitted
[14] Meijerink A, Nuyten J and Blasse G 1989 *J. Lumin.* **44** 19–31
[15] Verwey J W M, Dirksen G J and Blasse G 1992 *J. Phys. Chem. Solids* **53** 367–75
[16] van der Kolk E, Dorenbos P, van Eijk C W E, Vink A P, Fouassier C and Guillen G 2001 *J. Lumin.* submitted
[17] Dorenbos P 2000 *Phys. Rev.* B **62** 15 640–9
[18] Dorenbos P 2000 *Phys. Rev.* B **62** 15 650–9
[19] Dorenbos P 2000 *J. Lumin.* **91** 91–106
[20] Collongues R, Lejus A M, Thery J and Vivien D 1993 *J. Cryst. Growth* **128** 986
[21] Aubert J J, Lejus A M, Viana B and Vivien D 1987 *European Patent Specification* 874013295
[22] Lindop A J, Matthews C and Goodwin D W 1975 *Acta Crystallogr.* B **31** 2940–1
[23] Perloff A and Block S 1966 *Acta Crystallogr.* **20** 274–9
[24] Guillot-Noël O, de Haas J T M, Dorenbos P and van Eijk C W E 1999 *J. Lumin.* **85** 21–35
[25] Zimmerer G 1991 *Nucl. Instrum. Methods Phys. Res.* **308** 178–86
[26] Elias L R, Heaps W S and Yen W M 1973 *Phys. Rev.* B **8** 4989–95
[27] Knitel M J, Dorenbos P, van Eijk C W E, Plasteig B, Viana B, Kahn-Harari A and Vivien D 2000 *Nucl. Instrum. Methods Phys. Res.* A **443** 364–74
[28] Mayolet A 1995 Etude des processus d'absorption et de transfert d'enerie au sein de materiaux inorganiques luminescents dan le domaine UV et VUV *PhD Thesis* Universite de Paris XI, Orsay
[29] Verstegen J M P J 1974 *J. Electrochem. Soc.* **121** 1623–7
[30] Stevels A L N 1978 *J. Electrochem. Soc.* **125** 588
[31] Koike J, Kojima T, Toyonaga R, Kagami A, Hase T and Inaho S 1979 *J. Electrochem. Soc.* **126** 1008–10
[32] Visser R, Dorenbos P, van Eijk C W E, Meijerink A, Blasse G and den Hartog H W 1993 *J. Phys.: Condens. Matter* **5** 1659–80
[33] van't Spijker J C, Dorenbos P, van Eijk C W E, Krāmer K and Güdel H U 1999 *J. Lumin.* **85** 1–10
[34] Okamoto S, Kobayashi H and Yamamoto H 1999 *J. Appl. Phys.* **86** 5594–7
[35] Schipper W J and Blasse G 1994 *J. Lumin.* **59** 337
[36] Srivastava A M and Duclos S J 1997 *Chem. Phys. Lett.* **275** 453–6
[37] van't Spijker J C, Dorenbos P, van Eijk C W E, Jacobs J E M, den Hartog H W and Korolev N 1999 *J. Lumin.* **85** 11–19
[38] Song K S and Williams R T 1993 *Self-Trapped Excitons (Springer Series in Solid-State Science)* (Berlin: Springer)
[39] van Dijk J M F and Schuurmans M F H 1983 *J. Chem. Phys.* **78** 5317–23

[40] Malinowski M, Woliński W, Wolski R and Strek W 1991 *J. Lumin.* **48+49** 235–8
[41] Balda R, Fernández J, Saéz de Ocáriz I, Voda M, García A J and Khaidukov N 1999 *Phys. Rev.* B **59** 9972–9
[42] Dornauf H and Heber J 1980 *J. Lumin.* **22** 1–16
[43] Lorenzo A, Bausá L E and García Solé J 1995 *Phys. Rev.* B **51** 16 643–50
[44] Saubat B, Vlasse M M and Fouassier C 1980 *J. Solid State Chem.* **34** 271–7
[45] Abdullaev G K, Mamedov K S and Dzhafarov G G 1981 *Kristallografiya* **26** 837–40
[46] Srivastava A M and Beers W W *United States Patent Specification* 5,788,883
[47] Srivastava A M and Beers W W *European Patent Application* EP 0 798 361 A1
[48] Blasse G 1973 *Phys. Status Solidi* b **55** K131
[49] Fouassier C, Latourette B, Portier J and Hagenmüller P 1976 *Mater. Res. Bull.* **11** 933–8
[50] Dorenbos P 2001 *Phys. Rev.* B submitted